AGU PUBLICATIONS

JGR

Journal of Geophysical Research: Atmospheres

RESEARCH ARTICLE
10.1002/2016JD025164

Key Points:
- In the satellite record, anomalies in Pacific sector ice cover are in part compensated by anomalies of opposite sign in the Atlantic sector
- There is asymmetry in the mechanisms that link summer atmospheric circulation regimes and open water anomalies
- High open water years are always associated with warm summers, but low open water years can be driven by cool summers or southward advection

Correspondence to:
A. H. Lynch,
Amanda_Lynch@brown.edu

Citation:
Lynch, A. H., M. C. Serreze, E. N. Cassano, A. D. Crawford, and J. Stroeve (2016), Linkages between Arctic summer circulation regimes and regional sea ice anomalies, *J. Geophys. Res. Atmos.*, *121*, 7868–7880, doi:10.1002/2016JD025164.

Received 29 MAR 2016
Accepted 28 JUN 2016
Accepted article online 2 JUL 2016
Published online 12 JUL 2016

Linkages between Arctic summer circulation regimes and regional sea ice anomalies

Amanda H. Lynch[1,2], Mark C. Serreze[3], Elizabeth N. Cassano[4], Alex D. Crawford[3], and Julienne Stroeve[3,5]

[1]Institute at Brown for Environment and Society, Brown University, Providence, Rhode Island, USA, [2]Department of Earth, Environmental and Planetary Sciences, Brown University, Providence, Rhode Island, USA, [3]National Snow and Ice Data Center, University of Colorado Boulder, Boulder, Colorado, USA, [4]Cooperative Institute for Research in Environmental Sciences, University of Colorado Boulder, Boulder, Colorado, USA, [5]Department of Earth Sciences, University College London, London, United Kingdom

Abstract The downward trend in overall Arctic summer sea ice extent has been substantial, particularly in the last few decades. Departures in ice extent from year to year can be very large, however, in part due to the high variability in summer atmospheric circulation patterns. Anomalies in the Pacific sector ice cover can be partially compensated by anomalies of opposite sign in the Atlantic sector. An assessment of linkages between summer atmospheric patterns and sectoral anomalies in the area of maximum open water north of 70°N demonstrates that there is asymmetry in the mechanisms. Years with low ice extent and high open water fraction are uniformly associated with positive temperature anomalies and southerly flow in both the Atlantic and Pacific sectors. However, years with high extent and low open water fraction in both sectors reveal two dominant mechanisms. Some years with anomalously low maximum open water fraction are associated with negative temperature anomalies and southerly transport—a cool summer pattern that allows ice to persist over larger areas. However, other low open water years are characterized by an "ice factory" mechanism, whereby—even when melting—ice cover is continually replenished by advection from the north.

1. Introduction

The global climate is a "complex agent of change in the Arctic" [*Lynch et al*., 2004], and nowhere is this better exemplified than at the sea ice margins. The sharp decline in end-of-summer Arctic sea ice extent over the period of satellite observations has attracted widespread attention [*Stroeve et al*., 2007; *Comiso et al*., 2008; *Kwok and Rothrock*, 2009; *Parkinson and Comiso*, 2013]. *Stroeve et al*. [2007] first noted that the decline in September ice extent was more rapid than expected from hindcasts based on the coupled climate models participating in the Intergovernmental Panel of Climate Change (IPCC) Fourth Assessment report. While there is better agreement with the newer models that participated in the IPCC Fifth Assessment, as a group, these models still have difficulty in capturing the observed retreat [*Stroeve et al*., 2012]. Indeed, the lowest nine September sea ice extents in the satellite records have all occurred in the past 9 years [*Fetterer et al*., 2010].

It is well known that the atmospheric circulation patterns play an important role in determining ice edge variability [*Serreze et al*., 1995; *Maslanik et al*., 2000; *Ogi and Wallace*, 2012; *Mills and Walsh*, 2014]. The surface wind largely drives the sea ice circulation, affecting, for example, whether the ice motion is offshore or onshore, and the overall thickness distribution. It also influences whether the ice motion is divergent or convergent [e.g., *Thorndike and Colony*, 1982; *Serreze et al*., 1989; *Arbetter et al*., 2004]. Atmospheric circulation variability also has thermodynamic influences, manifested in factors such as ice melt and growth rates. These two components of atmospheric forcing may reinforce each other. For example, anomalous southerly winds may lead to offshore ice motion, leaving areas of open water along the coast, and southerly winds are also warm winds, which can accentuate summer melt. Further, wind-generated mixing of the upper ocean has a dramatic effect on basal melting [*Richter-Menge et al*., 2001] and surface ocean temperatures [*Saetra et al*., 2008]. On longer time scales, the influence becomes more significant as polar lows spin up the Nordic Seas gyre, enhancing the depth, frequency, and area of deep convection in the Nordic seas, which in turn leads to a larger northward transport of heat into the region, and southward transport of deep water through Denmark Strait, enhancing Arctic Ocean ice export by up to 20% [*Condron et al*., 2006]. The forcing can also go the other way. For example, the marginal sea ice influences the surface baroclinicity, leading to a modulation in polar low activity at the ice edge [*Lynch et al*., 2003; *Tsukernik et al*., 2007; *Bracegirdle and Gray*, 2008].

Studies of linkages between atmospheric circulation patterns and the downward trend in annual Arctic sea ice minimum have suggested systematic relationships between low sea ice years and patterns of atmospheric variability including the Arctic Oscillation (AO) [*Ogi and Wallace*, 2007], the Arctic Dipole anomaly [*Wu et al*., 2006; *Overland et al*., 2012] and more regionally inhomogeneous signals [*Ukita et al*., 2007]. While the first-order downward trend in September Arctic sea ice extent has been strong [*Deser et al*., 2000], particularly in the last few decades, departures in ice extent from year to year can be very large, exceeding 1.0×10^6 km^2 in considerable part because of strong variability in summer atmospheric circulation patterns [*Serreze and Stroeve*, 2015]. A good example is the contrast between the record low September extent observed in 2012 (3.49×10^6 km^2) associated with warm conditions and the strong recovery in 2013 (5.35×10^6 km^2) when a relatively cool and cyclonic atmospheric pattern prevailed. However, years with very different patterns of summer atmospheric circulation can also yield very similar total September ice extent, when circulation-induced anomalies in extent in one region of the Arctic are compensated by anomalies of opposite sign in another, a good example being the year 2013. A relevant conclusion of that paper is that while there is merit in relating variability in total September ice extent to modes of variability such as the summer AO and the Arctic Dipole anomaly, such frameworks are limited because even minor differences in the location and strength of summer atmospheric circulation anomalies can lead to very different patterns of sea ice drift and air temperature anomalies.

In the present study, we perform a rigorous assessment of linkages between summer atmospheric patterns and regional anomalies in sea ice extent for each the Atlantic and Pacific sectors of the Arctic using the self-organizing map (SOM) framework. By separating the analyses into two sectors, we seek to filter out sectoral covariability [e.g., *Ukita et al*., 2007; *Yang and Yuan*, 2014] or annular character [e.g., *Rigor et al*., 2002] in order to focus on the details of linkages between regional atmospheric forcing and sea ice.

2. Data Sets and Methodology

2.1. Ice Area

The data source is daily sea ice extent from the combined Nimbus Scanning Multichannel Microwave Radiometer (SMMR, July 1979 to September 1986), the Defense Meteorological Satellite Program (DMSP) Special Sensor Microwave/Imager (SSM/I, July 1987 to September 2007) and the Special Sensor Microwave Imager/Sounder (SSMIS, July 2008 to September 2014) 25 km gridded sea ice concentration data product from the NASA Team sea ice algorithm [*Cavalieri et al*., 1996], which is distributed by the National Snow and Ice Data Center.

Monthly mean open water area was calculated separately for the Atlantic and Pacific sectors of the Arctic. These sectors were divided by the 100°E and 100°W meridians and bounded on the south by the 70°N parallel. From each daily sea ice concentration field, the open water area of each sector was calculated as the area of grid cells for which sea ice concentration was less than or equal to 15%. The monthly mean for each July, August, and September for the period 1979 to 2014 was obtained from these daily values. Next, the 36 year time series for each sector month was detrended, and these detrended values were then standardized according to

$$\mathbf{A_z} = \left(\mathbf{A_d} - \bar{A}_d\right)/\boldsymbol{\sigma}$$

where $\mathbf{A_d}$ is the vector of detrended open water areas, $\bar{A}_d$ and $\boldsymbol{\sigma}$ are the mean and standard deviation of $\mathbf{A_d}$, respectively, and $\mathbf{A_z}$ is the vector of standardized detrended open water areas. The effect of detrending will be discussed in more detail section 3a.

2.2. Regional Circulation

We use a SOM framework that sorts the atmospheric circulation into regimes [*Hewitson and Crane*, 2002; *Cassano et al*., 2006]. As noted in *Cassano et al*. [2006], the SOM may be described as "a non-linear mapping of high-dimensional input data onto the elements of a regular low dimensional array". This array is constructed by presenting a neural network with a set of vectors—constructed by appending each row of each input matrix into a single row—that are classified according to their Euclidean distance from a characteristic node vector and sorted so as to be representative of the probability density function of the input data. In this application, the SOM algorithm places the distribution of input data into a 5×4 array of nodes. The number of nodes selected dictates how much intranode spread will be represented by the classes. More nodes will produce a broader range of patterns with more gradual differences between them, while fewer nodes will result

Table 1. Linear Regression Statistics for the Arctic, the Pacific, and Atlantic Sectors, and a Number of the Regional Seas[a]

Region	Trend (Percent Open Area Per Decade)	SD (%)	Standard Error	Coefficient of Variation	Residual Sum of Squares
Arctic Region, north of 70°N	5.2	6.4	0.06	0.71	0.04
Central Arctic Ocean	2.0	3.9	0.05	0.29	0.04
Pacific Sector	9.1	11.7	0.11	0.65	0.17
Atlantic Sector	2.1	3.4	0.04	0.42	0.02
Bering Sea	0.1	0.1	0.0	0.72	0.0
Beaufort Sea	12.0	18.5	2.3	0.45	0.67
Chukchi Sea	16.0	20.5	0.20	0.66	0.52
East Siberian Sea	17.2	24.7	0.28	0.53	1.04
Laptev Sea	13.4	21.8	0.28	0.41	1.01
Kara Sea	7.8	14.8	0.20	0.30	0.55
Barents Sea	0.8	2.8	0.04	0.09	0.03
GINI Seas	1.1	3.2	0.05	0.14	0.03
Baffin Bay and Labrador Sea	0.5	0.9	0.01	0.25	0.0

[a]The GINI Seas represents the Greenland, Irminger, Norwegian, and Iceland Seas.

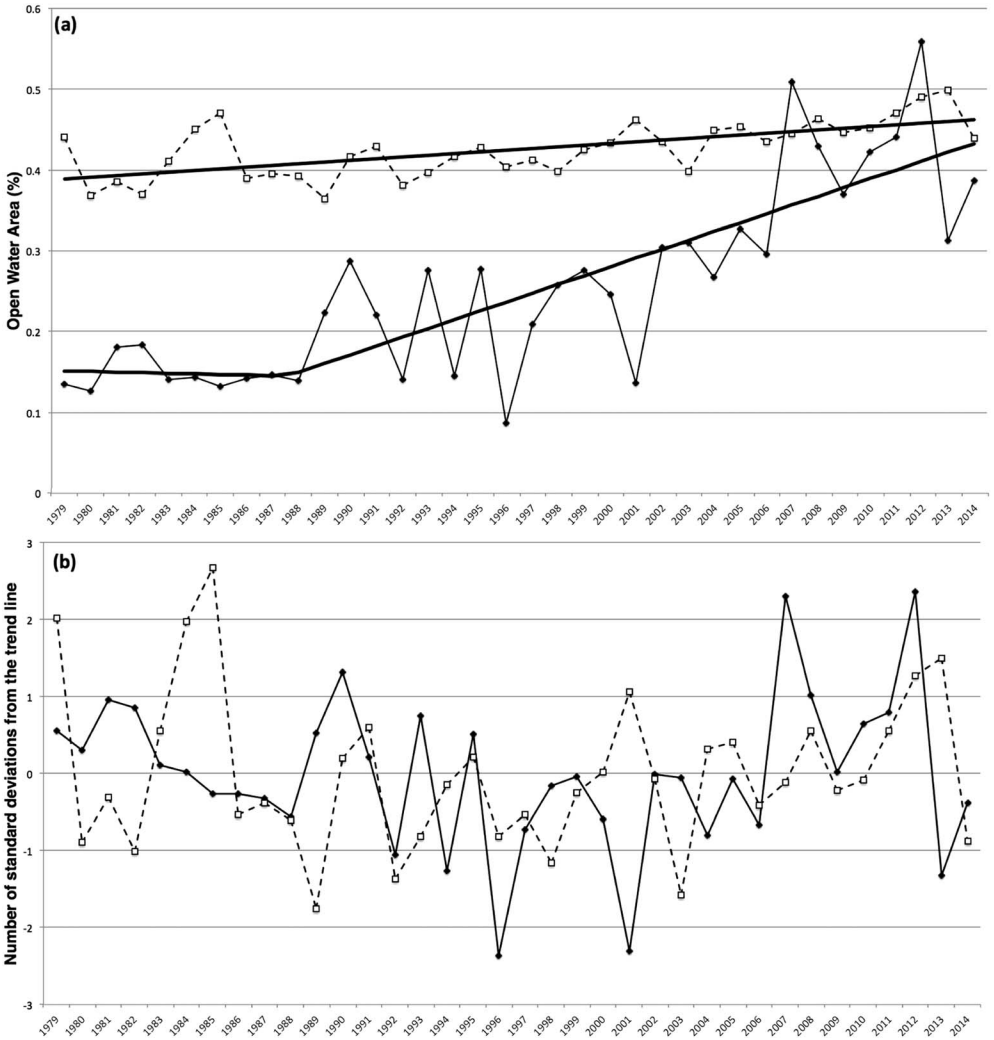

Figure 1. Pacific (100°E–100°W; solid) and Atlantic (100°W–100°E; dashed) sectors September open water fraction from the combined Nimbus SMMR and DMSP SSM/I-SSMIS 25 km product from 1979 to 2014. (a) September open water (fraction of area less than 15% concentration). (b) Departures from the trend in open water area (number of standard deviations).

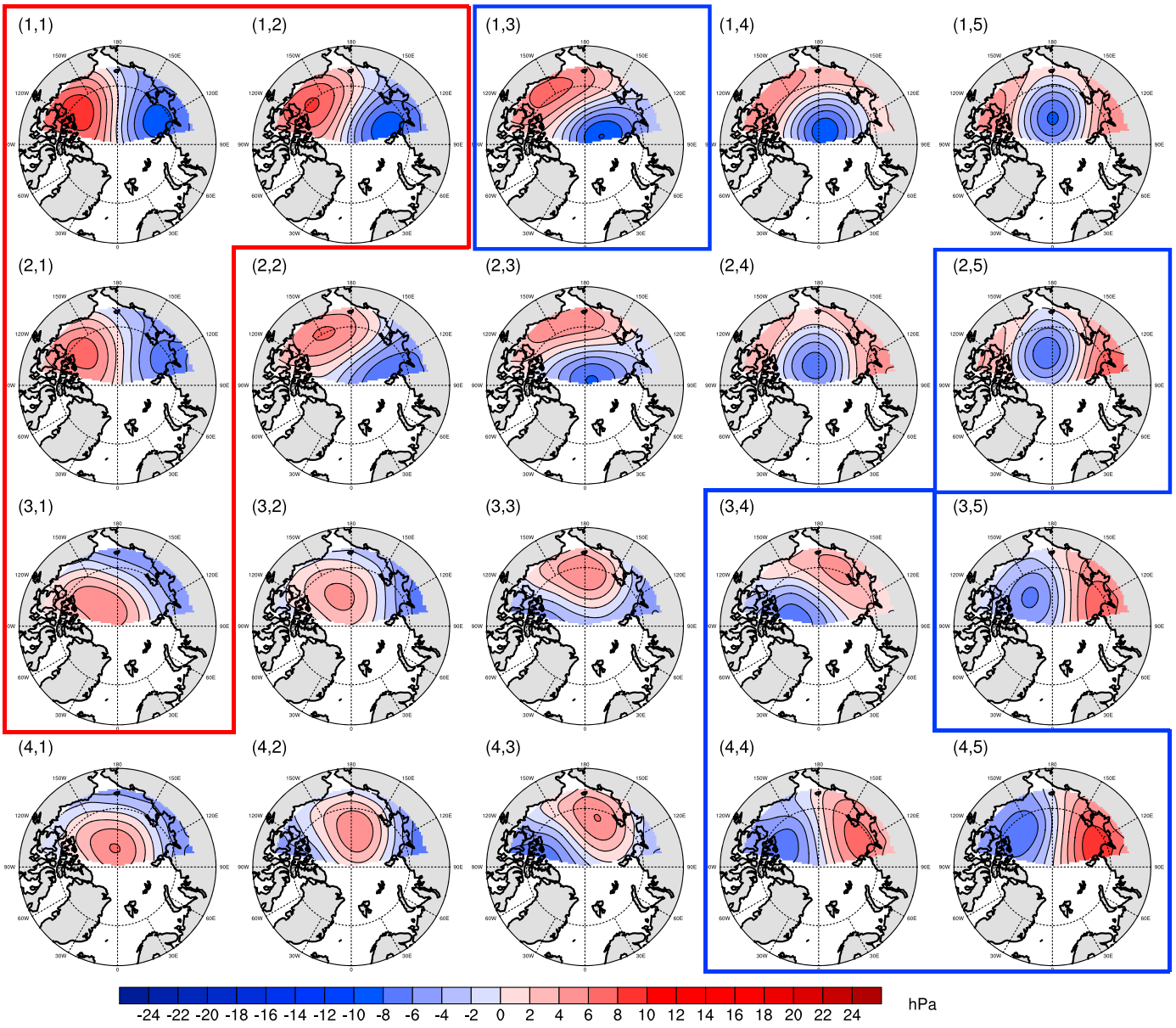

Figure 2. Pacific sector July through September sea level pressure anomalies (hPa) mapped to a 5 × 4 self-organizing map. The nodes outlined in red are circulation types most frequently associated with extremely high open water in September (more than 1.5 standard deviation from the mean) in the Pacific sector. The nodes outlined in blue are circulation types most frequently associated with extremely low open water (less than −1.5 standard deviation from the mean) in the Pacific sector.

in both larger intranode and internode spread, though the same broad patterns will be revealed in each case. Twenty nodes were selected for this analysis as this size gives a balance between a pragmatic minimum of patterns and sufficient patterns to characterize the range of variability of interest for this analysis. Separate analyses were performed for the Pacific and Atlantic sectors of the Arctic.

This application uses the ERA-Interim [*ECMWF*, 2009; *Dee et al.*, 2011] daily mean sea level pressure (SLP) anomaly data for 1979–2014, interpolated to the 50 km EASE grid. This is congruent with the Arctic-wide SOM of *Mills and Walsh* [2014], and our approach was verified by reproducing this SOM (not shown.) However, for the present paper, we only analyze the circulation for the months July, August, and September. Daily SLP anomalies were calculated by subtracting each day's domain-averaged SLP from the grid point value for that same day. Anomaly data were used rather than absolute values. This is justified in that anomaly gradients of SLP are most relevant for determining variations the near-surface circulation that

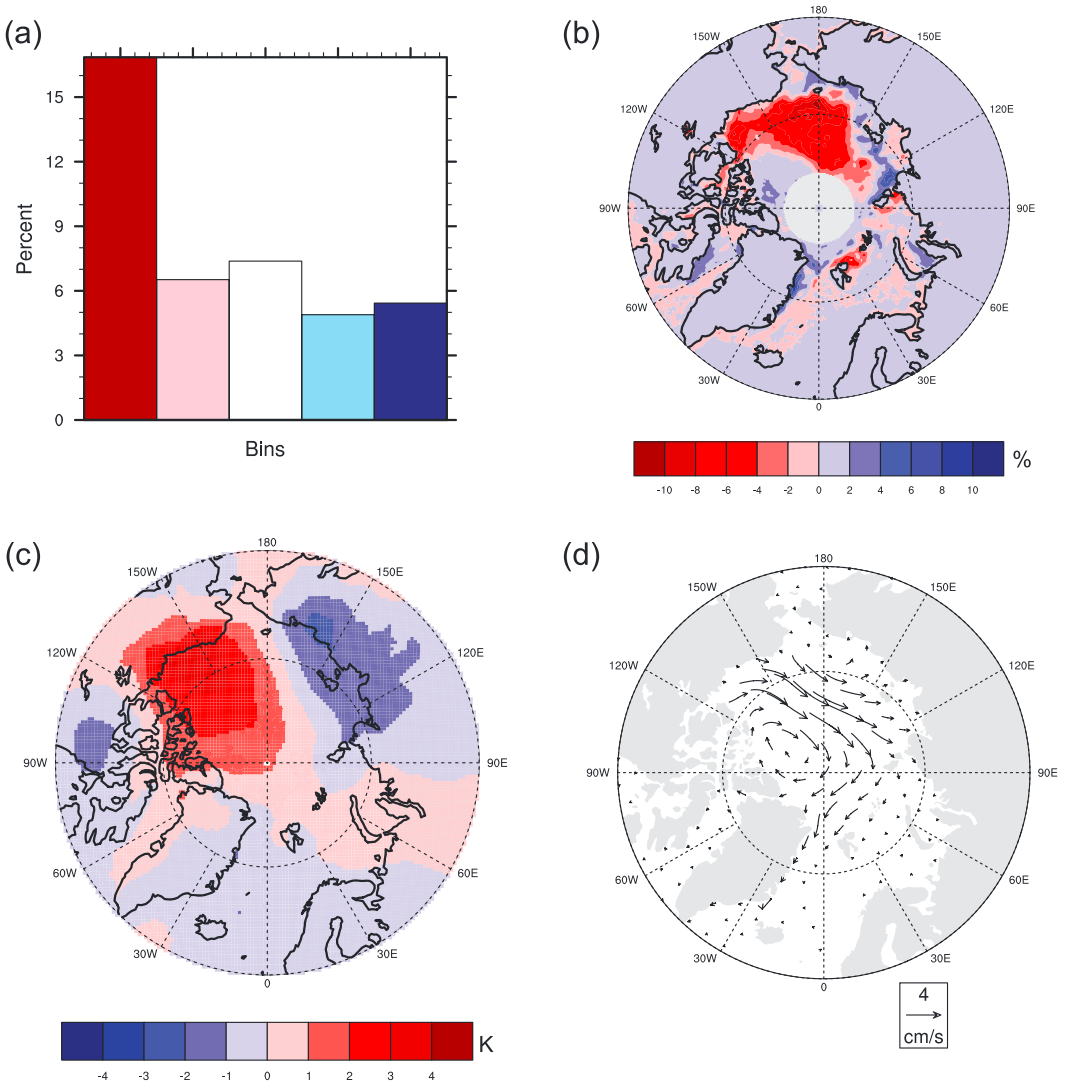

Figure 3. Fields corresponding to Node (3, 1) of the SOM pictured in Figure 2. As described in section 2b, these fields are found by finding the mean of each field associated with the days assigned to that node in the SOM. This node represents the circulation that occurs with most frequency over the summer that results in an extreme (greater than 1.5 standard deviation) high September open water. (a) Frequency analysis of open water. The bars represent detrended open water area classes ranging from greater than 1.5 standard deviations (dark red), between 0.5 and 1.5 standard deviation (light red), between 0.5 and −0.5 standard deviation (white), between −0.5 and −1.5 standard deviation (light blue), and less that −1.5 standard deviation (dark blue). (b) Daily sea ice area anomalies (%), (c) 925 hPa temperature daily anomalies (K), and (d) mean ice vectors (cm/s).

are of primary interest. Grid points with elevations >500 m (that is, over Greenland) were filtered from the SOM analysis due to errors associated with reducing surface pressure to SLP for high-elevation locations [*Mohr*, 2004; *Wallace and Hobbs*, 2006].

Once the SOM is trained, each input sample day is assigned to the node it most closely matches. This results in a list of days that map to each node, and this list is used to map other data to the node. In this context, use is made of air temperature at the 925 hPa level, gridded sea ice area (see previous section), and gridded sea ice motion data. Temperature data are obtained from the ERA-Interim data set. The 925 hPa air temperature is preferred over the 2 m temperature because it provides a much better indicator of lower tropospheric warmth—over a melting ice surface the 2 m temperature will not vary much from the melting point. The sea ice motion vectors are from the Polar Pathfinder Daily 25 km EASE grid data set available from the National Snow and Ice Data Center [*Fowler et al.*, 2013].

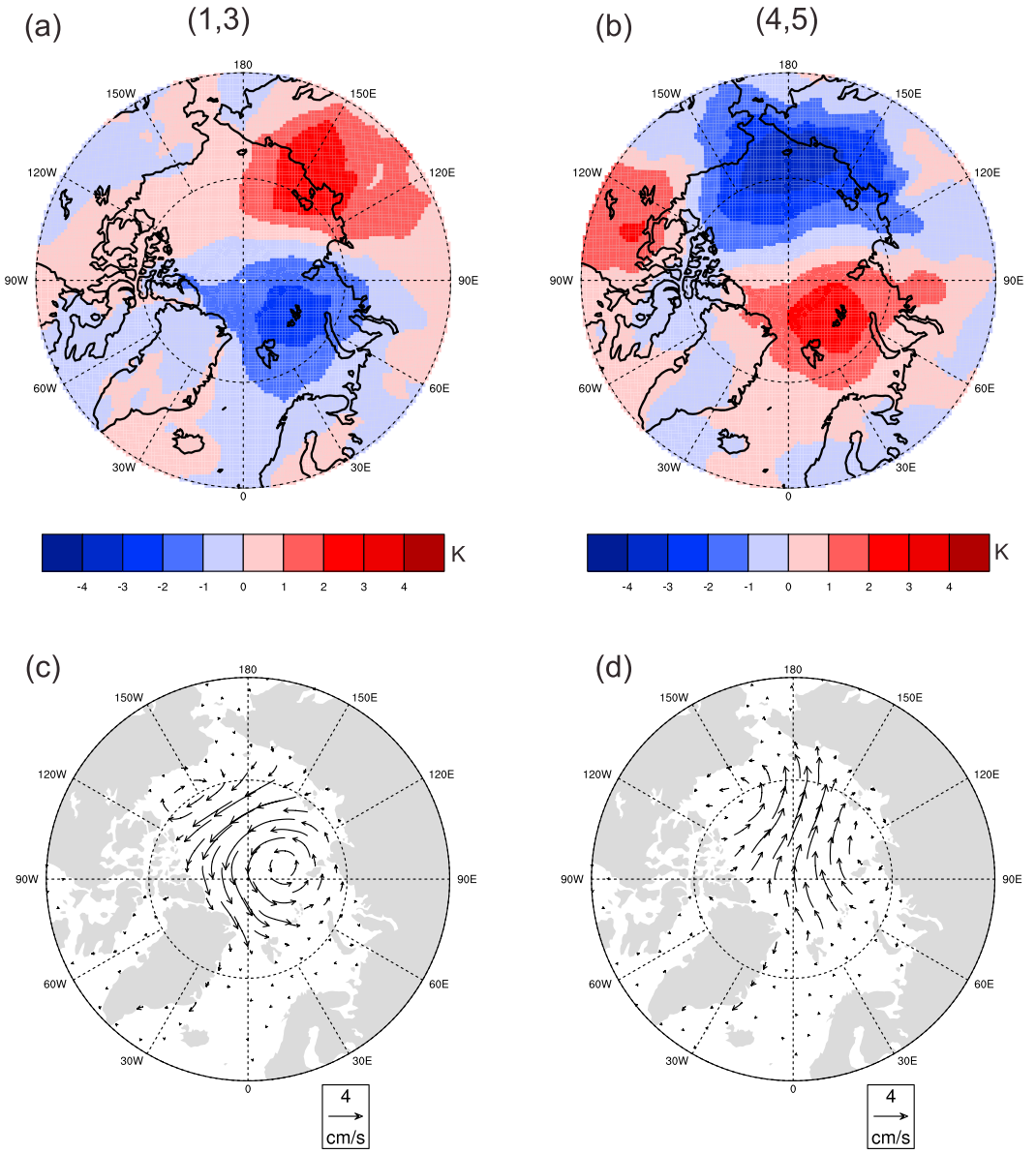

Figure 4. Fields corresponding to Nodes (1, 3) and (4, 5) of the SOM pictured in Figure 2, calculated as for Figure 3. These nodes represent the circulations that occur with most frequency over the summer that result in an extreme (greater than 1.5 standard deviation) low September open water. Shown are 925 hPa temperature daily anomalies (K) for (a) Node (1, 3) and (b) Node (4, 5), and mean ice vectors (cm/s) for (c) Node (1,3) and (d) Node (4,5).

3. Results

3.1. Sectoral Trends in Open Water

As assessed over the period 1979–2014, the upward trend in the September open water fraction is larger in the Pacific sector (9% per decade) than over the Atlantic sector (trend of 2% per decade) (Table 1 and Figure 1a). The smaller Atlantic-side trend is due in part to the ubiquity of Fram Strait export maintaining some measure of ice cover in that sector [e.g., *Smedsrud et al*., 2016], although as Table 1 demonstrates, the trends in variability are small in all but the Kara Sea on the Atlantic side. Indeed, the variability in open water fraction in the Pacific sector is more than an order of magnitude greater than in than the Atlantic sector. Finally, it is apparent that the Arctic-wide departures in summer open water fraction from year to year are typically the result of large and—at least before 2009—partially compensating regional anomalies between the Atlantic

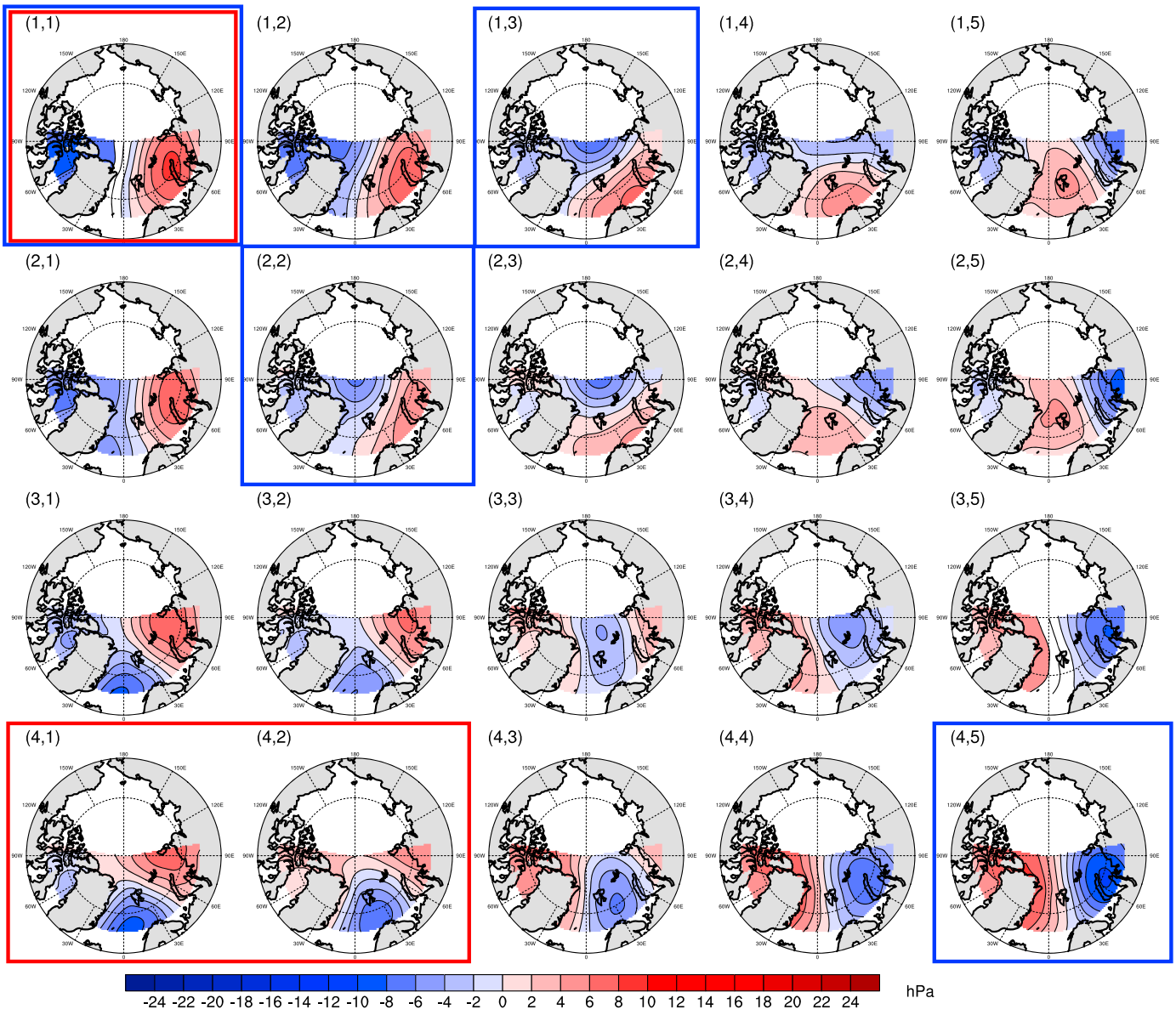

Figure 5. Atlantic sector July through September sea level pressure anomalies (hPa) mapped to a 5 × 4 self-organizing map. The nodes outlines in red are circulation types most frequently associated with extremely high September open water (more than 1.5 standard deviation from the mean) in the Atlantic sector. The nodes outlined in blue are circulation types most frequently associated with extremely low September open water (less than −1.5 standard deviation from the mean) in the Atlantic sector.

and Pacific sectors (Figure 1b). It is clear that the drivers of ice variability in the Pacific sector are different from the drivers in the Atlantic sector, and indeed it is likely that the dominant scales of variability may be smaller than the sectoral perspective used here.

Caution is called for in interpreting linear regressions, however. It can be demonstrated that a statistical model characterized by a series of breakpoints (difference in the means) is more statistically significant than a model characterized by a linear trend in the Pacific sector [*Goldstein et al.*, 2016]. The breakpoints occur in 1988 and (more weakly significantly) in 2007. That a "three-mean" model is more significant than a linear trend model is apparent in both NASA Team and Bootstrap algorithm records, as well as derived records such as ice age, and quasi-independent records such as the operational ice charts. In the Atlantic sector, this model could also be argued to be marginally significant [*Goldstein et al.*, 2016].

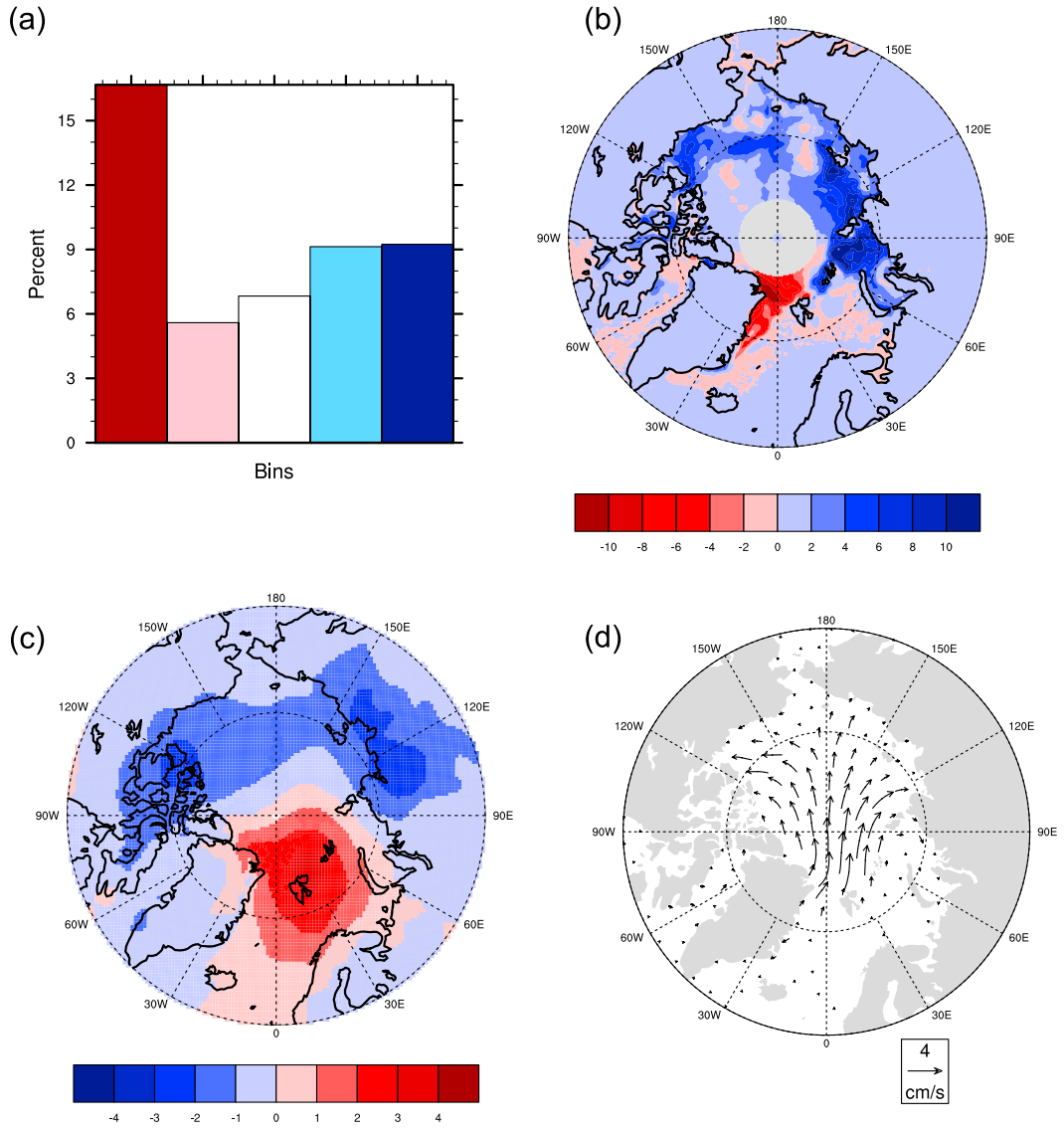

Figure 6. Fields corresponding to Node (1, 1) of the SOM pictured in Figure 5, calculated as for Figure 3. (a) Frequency analysis of open water. The bars represent detrended open water area classes ranging from greater than 1.5 standard deviations (dark red), between 0.5 and 1.5 standard deviation (light red), between 0.5 and −0.5 standard deviation (white), between −0.5 and −1.5 standard deviation (light blue), and less that −1.5 standard deviation (dark blue). (b) Daily sea ice area anomalies (%), (c) 925 hPa temperature daily anomalies (K), and (d) mean ice vectors (cm/s).

3.2. Sectoral Relationships Between Circulation and Ice

Figure 2 shows Pacific sector SLP anomalies for the months July through September mapped to a 5 × 4 SOM. Variability in the summer circulation appears as dominant cyclonic (e.g., Node (1, 5)) and anticyclonic (e.g., Node (4, 2)) circulation, as well as dipole (opposite sign) patterns, which include a Beaufort Sea high paired with a Laptev Sea low (e.g., Node (1, 1)) and a Beaufort Sea low paired with a Laptev Sea high (e.g., Node (4, 5)). An important feature of the SOM approach is that the less similar pairs of circulation patterns are in terms of Euclidean distance between the vectors formed by two SLP arrays, the further apart they will be placed on the map.

The top left hand sector of the SOM in Figure 2 is outlined in red. This set of four circulation regimes—characterized by a Beaufort Sea High and a Laptev Sea low—are associated statistically significantly with positive anomalies of open water, southerly advection of ice, and positive anomalies in 925 hPa temperatures. The most extreme low ice years correspond to a high frequency of occurrence of the circulation regime depicted

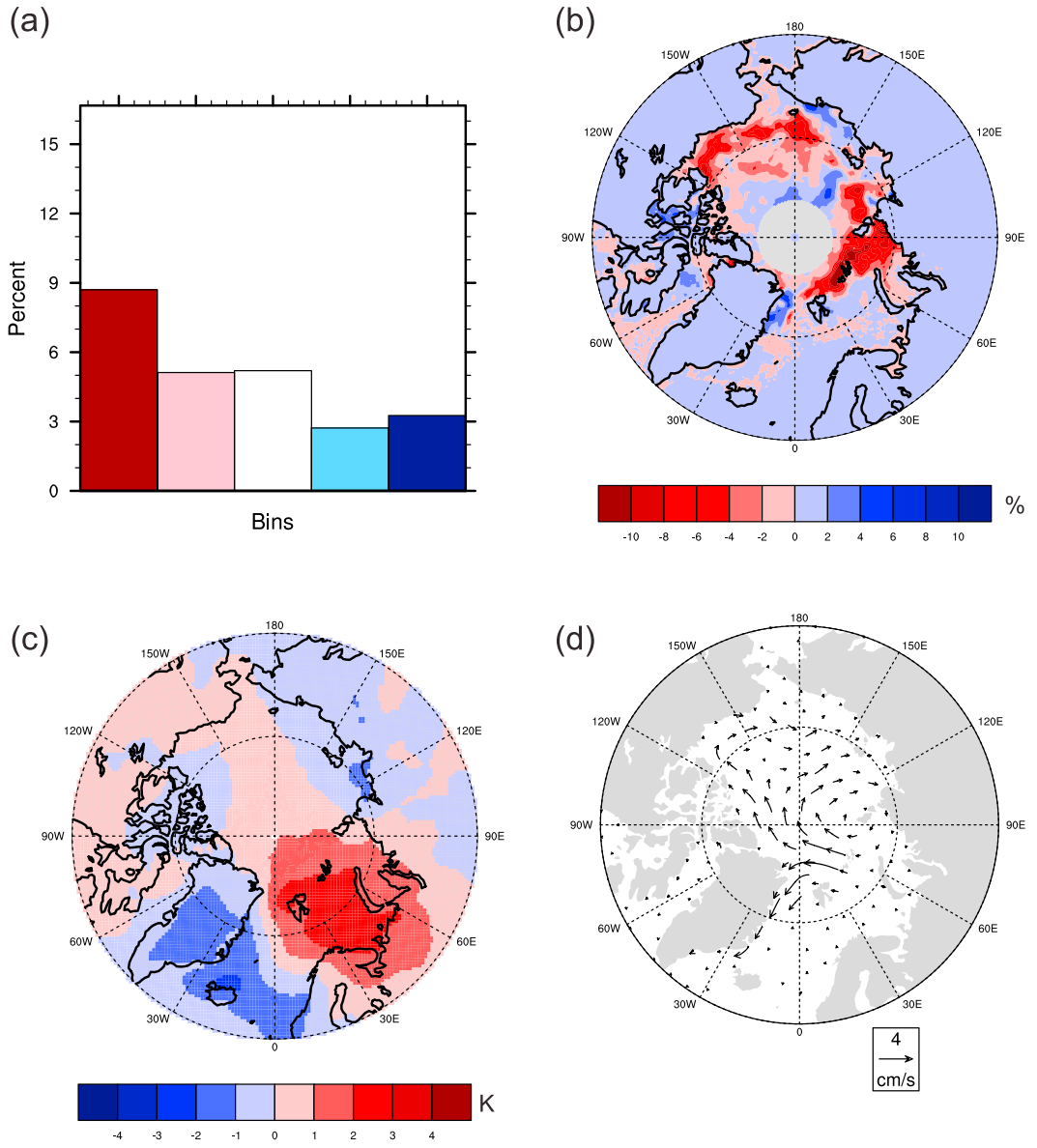

Figure 7. Fields corresponding to Node (4, 1) of the SOM pictured in Figure 5, calculated as for Figure 3. (a) Frequency analysis of open water. The bars represent detrended open water area classes ranging from greater than 1.5 standard deviations (dark red), between 0.5 and 1.5 standard deviation (light red), between 0.5 and −0.5 standard deviation (white), between −0.5 and −1.5 standard deviation (light blue), and less that −1.5 standard deviation (dark blue). (b) Daily sea ice area anomalies (%) and (c) 925 hPa temperature daily anomalies (K). (d) Mean ice vectors (cm/s).

in Node (3, 1) (Figure 3), which is characterized by warm southerlies originating over Canada and Alaska, attended by negative open water anomalies along the Siberian coast and low snow extent in the Canadian Arctic (not shown). These Siberian open water anomalies are known to be associated with the suppression of cyclonic activity in the Beaufort sea [*Lynch et al*., 2003], and hence, this regime may be self-reinforcing. Years with positive anomalies in open water predominate during summers featuring synoptic regimes that are congruent with the *Overland et al*. [2012] Arctic Dipole and the *Mills and Walsh* [2014] Beaufort High/Eurasian Low nodes. They also argue that these synoptic situations promote the evacuation of ice from the Canadian sector.

In contrast to the consistent character of high open water years, low open water years in the Pacific sector are associated with a range of circulation regimes (outlined in blue in Figure 2). This finding that open water

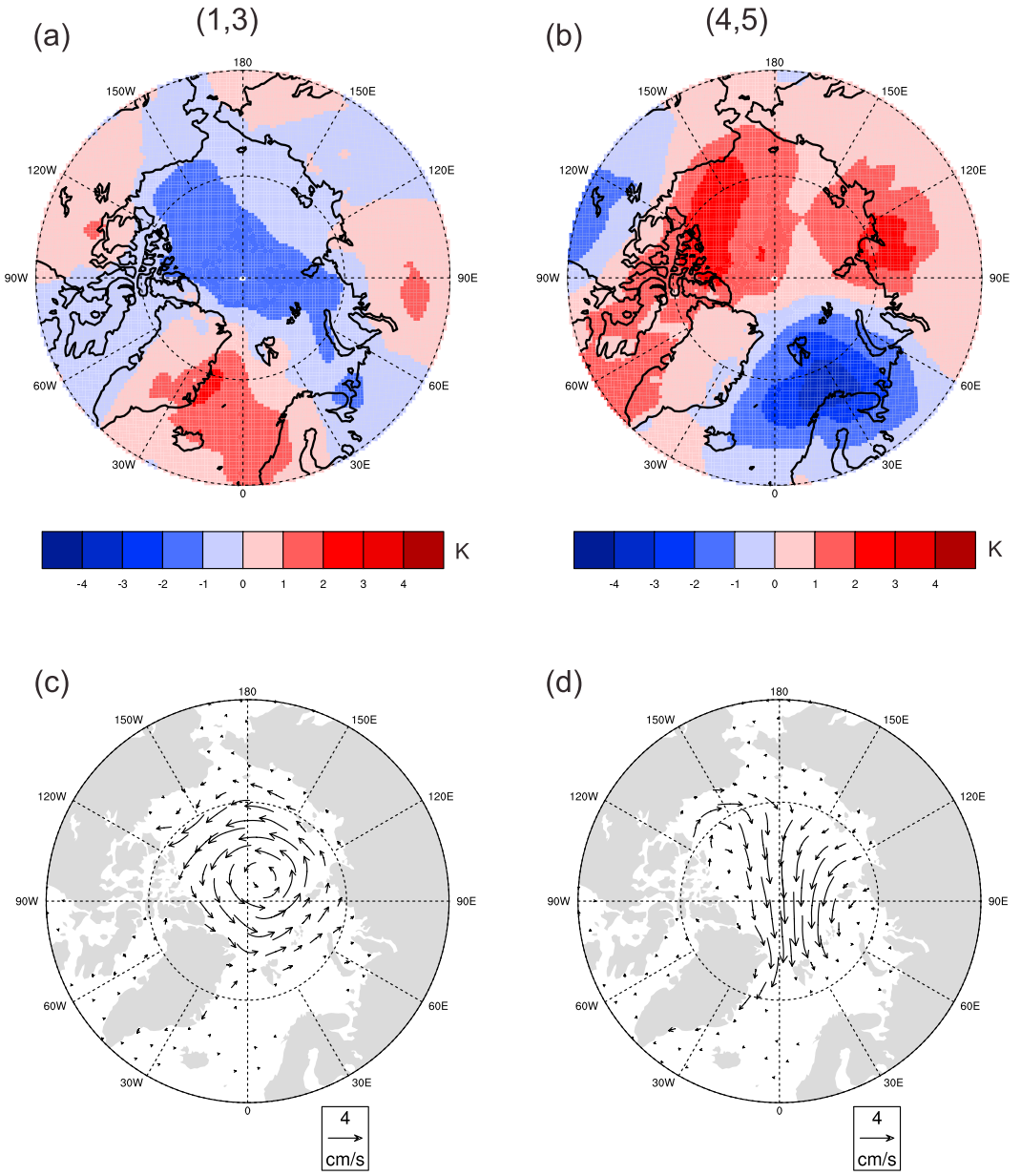

Figure 8. Fields corresponding to Nodes (1, 3) and (4, 5) of the SOM pictured in Figure 5, calculated as for Figure 3. These nodes represent the circulations that occur with most frequency over the summer that result in an extreme (less than −1.5 standard deviation) low September open water. Shown are 925 hPa temperature daily anomalies (K) for (a) Node (1, 3) and (b) Node (4, 5) and mean ice vectors (cm/s) for (c) Node (1, 3) and (d) Node (4, 5).

anomalies of the same sign arise from different circulation regimes is not reflected in research that explores teleconnections and correlations among binary modes [e.g., *Deser et al.*, 2000]. Low open water years do not typically overlap with the characteristic circulation regimes frequent in high open water, low ice, years, although as shown in Figure 3a extremely low open water years do occasionally correspond with a frequent occurrence of the circulation depicted in Node (3, 1). Two dominant categories of circulation are more typically associated with less open water and higher than average ice area: (i) warm southerly winds from the Siberian coast, promoting the poleward transport of ice away from the Chukchi coast and promoting cyclonic developments to the north, but allowing ice to concentrate in the Beaufort Sea and in the Canadian Archipelago (e.g., Node (1, 3); Figures 4a and 4c); and (ii) cold winds from the north leading to an increase in ice area along the Siberian coast, although in most cases the Beaufort ice cover is around average, unless a large central Arctic low dominates for some period of time (e.g., Node (4, 5), Figures 4b and 4d).

Similar to the Pacific SOM, the Atlantic sector summer circulation consists (Figure 5) broadly of a dominant Norwegian cyclone (consistent with the positive phase of the North Atlantic Oscillation, e.g., Node (4, 2)) and anticyclone (consistent with negative phase of the North Atlantic Oscillation, e.g., Node (1, 5)), as well as dipole patterns of opposite sign, which include a Barents Sea high and Greenland Sea low (e.g., Node (1, 1)) and Barents Sea low and Greenland Sea high (e.g., Node (4, 5)).

As with the Pacific analysis, the circulation regimes that occur most frequently over the summer preceding anomalously low (high) September ice extent are outlined in red (blue). Node (1, 1) is outlined in both blue and red because this circulation regime occurs frequently for extremely high (greater than 1.5 standard deviation) open water years as well as extremely low (less than −1.5 standard deviation) open water years (Figure 6a). This is a situation where a SOM with a greater number of patterns might be able to separate this node into two patterns reflecting small shifts in the circulation, and indeed this node does have a high intranodal spread. However, adopting a higher dimensionality would also add excessive detail to other parts of the map. Average ice years are more typical when the circulation regime is dominated by Nodes (1, 4), (1, 5), and (2, 5).

The ice extent, ice transport and 925 hPa air temperature anomaly characteristics typically associated with the Node (1, 1) pattern are shown in Figure 6. This node is associated with a warmer than average Atlantic sector, with positive anomalies stretching from the Barents Sea through the Norwegian and Greenland Seas. Sea ice extent is lower than average on the Greenland side and higher than average on the Barents Sea side, with an anomalous northward advection of ice through Fram Strait. In the years with extremely low September ice cover, the balance of this pattern yields anomalously low ice extent throughout the Greenland Sea and northward to the pole. Anomalous high ice extent in the Barents Sea has a small latitudinal range. For the years with somewhat higher ice cover, the Barents Sea ice stretches northward to the pole and westward to Svalbard and sometimes slightly beyond.

More consistently, low ice is exemplified by a high frequency of the circulation type depicted in Nodes (4, 1) (Figure 7) and (4, 2), ice export out of the anomalously warm Barents Sea and diverging, with one stream directed toward the Canadian Archipelago and the other stream directed southward along the east coast of Greenland. These years are also characterized by a negative phase of the North Atlantic Oscillation and a warm Fram Strait region.

As with the Pacific sector, high ice extent in the Atlantic sector is associated with two distinct mechanisms, illustrated by their large Euclidian distance on the SOM between Node (1, 3) and Node (4, 5). A warm North Atlantic and a cold Arctic with transport across Fram Strait keeps the Atlantic sector ice covered, although the anomalies are not large in the years where the synoptic situation is frequently characterized by Node (1, 3) (Figures 8a and 8c). Alternatively, a cold North Atlantic and marginal seas with strong cross Arctic transport and Fram Strait outflow, associated with a steep east to west pressure gradient, yields more extensive ice in this region as well as shown for Node (4, 5) (Figures 8b and 8c).

4. Conclusions

It is apparent that while the ice cover in the Arctic is retreating rapidly, the character of the changing ice is very different in the Atlantic and Pacific sectors. Even accounting for a possible shift in the mean of open water fraction in the Pacific sector, the trend toward more open water and less extensive ice in late summer is larger than in the Atlantic sector. Year to year variability in the open water fraction is also apparently larger in the Pacific sector. This different character is due in large part to the consistent export of ice maintaining a more extensive, and progressively thinner and newer, ice cover in the European Arctic peripheral seas.

Here we have found a strong asymmetry in the mechanisms that result in anomalously low or high September open water fraction. Not surprisingly, years that result in low ice extent and high open water fraction on both sides of the Arctic are uniformly associated with positive 925 hPa temperature anomalies and southerly flow, both melting ice and driving the summer ice that remains closer to the pole. However, for years that depart from the downward trend in ice extent toward more ice cover and less open water, (particularly those that are more than 1.5 standard deviations away from the trend), there are two different mechanisms. Some high ice years are associated with negative temperature anomalies and southerly transport—a cool summer pattern that allows ice to persist over larger areas. Some high ice years, on the other hand, are characterized by an "ice factory" mechanism, whereby ice cover is continually replenished by

advection from the north. We expect that these years would also be associated with lower than normal ice thickness than the cool summer patterns.

The intersection of sea ice variability with economic activity in the Arctic is no more apparent than in the ongoing quest for time-sensitive decision support for technically feasible navigation routes. The long-term trends point toward open water oil and gas infrastructure and navigable supply routes by 2040 [*Smith and Stephenson*, 2013]. However, the near-term intraseasonal variability of open water in the Arctic affects decisions around shipping routes, oil rig licensing, and emergency planning. Better understanding of the mechanisms that determine large departures from the long-term trend will provide an important scientific foundation for actionable knowledge at the ice edge.

Acknowledgments
This work was partially supported by a Visiting Fellowship from the Cooperative Institute for Research in Environmental Sciences and a research award from the Institute at Brown for Environment and Society. We acknowledge the National Snow and Ice Data Center for providing the sea ice data, which is freely available from http://www.nsidc.org and the European Centre for Medium-Range Weather Forecasts for providing the ERA-Interim data which are freely available at http://apps.ecmwf.int/datasets/. The authors acknowledge with thanks the technical support of Todd Arbetter and the useful discussions about data quality with Florence Fetterer.

References

Arbetter, T. E., A. H. Lynch, and D. A. Bailey (2004), Relationship between synoptic forcing and polynya formation in the Cosmonaut Sea: 1. Polynya climatology, *J. Geophys. Res.*, *109*, C04022, doi:10.1029/2003JC001837.

Bracegirdle, T. J., and S. L. Gray (2008), An objective climatology of the dynamical forcing of polar lows in the Nordic seas, *Int. J. Climatol.*, *28*(14), 1903–1919, doi:10.1002/joc.1686.

Cassano, E. N., A. H. Lynch, J. J. Cassano, and M. R. Koslow (2006), Classification of synoptic patterns in the western Arctic associated with extreme events at Barrow, Alaska, USA, *Clim. Res.*, *30*(2), 83–97, doi:10.3354/cr030083.

Cavalieri, D. J., C. L. Parkinson, P. Gloersen, and H. J. Zwally (1996), Sea ice concentrations from Nimbus-7 SMMR and DMSP SSM/I-SSMIS passive microwave data, Version 1. National Snow and Ice Data Center (NSIDC), Boulder, Colo.

Comiso, J. C., C. L. Parkinson, R. Gersten, and L. Stock (2008), Accelerated decline in the Arctic Sea ice cover, *Geophys. Res. Lett.*, *35*, L01703, doi:10.1029/2007GL031972.

Condron, A., G. R. Bigg, and I. A. Renfrew (2006), Polar mesoscale cyclones in the northeast Atlantic: Comparing climatologies from ERA-40 and satellite imagery, *Mon. Weather Rev.*, *134*(5), 1518–1533, doi:10.1175/mwr3136.1.

Dee, D. P., et al. (2011), The ERA-Interim reanalysis: configuration and performance of the data assimilation system, *Q. J. R. Meteorol. Soc.*, *137*(656), 553–597, doi:10.1002/qj.828.

Deser, C., J. E. Walsh, and M. S. Timlim (2000), Arctic sea ice variability in the context of recent atmospheric circulation trends, *J. Clim.*, *13*, 617–633.

European Centre for Medium-Range Weather Forecasts (2009), Updated monthly. *ERAI-Interim Project*. Research Data Archive at the National Center for Atmospheric Research, Computational and Information Systems Laboratory, doi:10.5065/D6CR5RD9.

Fetterer, F., M. Savoie, S. Helfrich, and P. Clemente-Colón (2010), Multisensor analyzed sea ice extent—Northern Hemisphere, National Ice Center (NIC) and National Snow and Ice Data Center (NSIDC), Boulder, Colo., doi:10.7265/N5GT5K3K.

Fowler, C., J. Maslanik, W. Emery, and M. Tschudi (2013), Polar pathfinder daily 25 km EASE-grid sea ice motion vectors. Version 2. Daily mean grids. National Snow and Ice Data Center (NSIDC), Boulder, Colo.

Goldstein, M. A., A. H. Lynch, T. E. Arbetter, and F. Fetterer (2016), Abrupt transitions in Arctic open water area, *Cryosphere Discuss.*, doi:10.5194/tc-2016-108.

Hewitson, B. C., and R. G. Crane (2002), Self-organizing maps: Applications to synoptic climatology, *Clim. Res.*, *22*(1), 13–26, doi:10.3354/cr022013.

Kwok, R., and D. A. Rothrock (2009), Decline in Arctic sea ice thickness from submarine and ICESat records: 1958–2008, *Geophys. Res. Lett.*, *36*, L15501, doi:10.1029/2009GL039035.

Lynch, A. H., E. N. Cassano, J. J. Cassano, and L. R. Lestak (2003), Case studies of high wind events in Barrow, Alaska: Climatological context and development processes, *Mon. Weather Rev.*, *131*, 719–732.

Lynch, A. H., J. A. Curry, R. D. Brunner, and J. A. Maslanik (2004), Toward an integrated assessment of the impacts of extreme wind events on Barrow, Alaska, *Bull. Am. Meteorol. Soc.*, *85*(2), 209–221, doi:10.1175/bams-85-2-209.

Maslanik, J. A., A. H. Lynch, M. C. Serreze, and W. Wu (2000), A case study of regional climate anomalies in the Arctic: Performance requirements for a coupled model, *J. Clim.*, *13*(2), 383–401.

Mills, C. M., and J. E. Walsh (2014), Synoptic activity associated with sea ice variability in the Arctic, *J. Geophys. Res. Atmos.*, *119*, 12,117–12,131, doi:10.1002/2014JD021604.

Mohr, M. (2004), Problems with the mean sea level pressure field over the western United States, *Mon. Weather Rev.*, *132*, 1952–1965.

Ogi, M., and J. M. Wallace (2007), Summer minimum Arctic sea ice extent and the associated summer atmospheric circulation, *Geophys. Res. Lett.*, *34*, L12705, doi:10.1029/2007GL029897.

Ogi, M., and J. M. Wallace (2012), The role of summer surface wind anomalies in the summer Arctic sea ice extent in 2010 and 2011, *Geophys. Res. Lett.*, *39*, L09704, doi:10.1029/2012GL051330.

Overland, J. E., J. A. Francis, E. Hanna, and M. Y. Wang (2012), The recent shift in early summer Arctic atmospheric circulation, *Geophys. Res. Lett.*, *39*, L19804, doi:10.1029/2012GL053268.

Parkinson, C. L., and J. C. Comiso (2013), On the 2012 record low Arctic sea ice cover: Combined impact of preconditioning and an August storm, *Geophys. Res. Lett.*, *40*, 6, doi:10.1002/grl.50349.

Richter-Menge, J. A., D. K. Perovich, and W. S. Pegau (2001), Summer ice dynamics during SHEBA and its effect on the ocean heat content, in *Annals of Glaciology*, vol. 33, edited by M. O. Jeffries and H. Eicken, pp. 201–206, Int Glaciological Soc., Cambridge, doi:10.3189/172756401781818176.

Rigor, I. G., J. M. Wallace, and R. L. Colony (2002), Response of sea ice to the Arctic Oscillation, *J. Clim.*, *15*(18), 2648–2663.

Saetra, O., T. Linders, and J. B. Debernard (2008), Can polar lows lead to a warming of the ocean surface?, *Tellus Dyn. Meteorol. Oceanogr.*, *60*(1), 141–153, doi:10.1111/j.1600-0870.2007.00279.x.

Serreze, M. C., and J. Stroeve (2015), Arctic sea ice trends, variability and implications for seasonal ice forecasting, *Philos. Trans. R. Soc. London, Ser. A*, *373*(2045), 16, doi:10.1098/rsta.2014.0159.

Serreze, M. C., R. G. Barry, and A. S. McLaren (1989), Seasonal variations in sea ice motion and effects on sea ice concentration in the Canada Basin, *J. Geophys. Res.*, *94*, 10,995–10,970, doi:10.1029/JC094iC08p10955.

Serreze, M. C., J. R. Maslanik, J. R. Key, R. F. Kokaly, and D. A. Robinson (1995), Diagnosis of the record minimum in Arctic sea ice area during 1990 and associated snow cover extremes, *Geophys. Res. Lett.*, *22*, 2183–2186, doi:10.1029/95GL02068.

Smedsrud, L. H., M. H. Halvorsen, J. C. Stroeve, R. Zhnag, and K. Kloster (2016), Fram Strait sea ice export variability and September Arctic sea ice extent over the last 80 years, *Cryosphere Discuss.*, doi:10.5194/tc-2016-79.

Smith, L. C., and S. R. Stephenson (2013), New Trans-Arctic shipping routes navigable by midcentury, *Proc. Natl. Acad. Sci. U.S.A.*, *110*(13), E1191–E1195, doi:10.1073/pnas.1214212110.

Stroeve, J., M. M. Holland, W. Meier, T. Scambos, and M. Serreze (2007), Arctic sea ice decline: Faster than forecast, *Geophys. Res. Lett.*, *34*, L09501, doi:10.1029/2007GL029703.

Stroeve, J. C., V. Kattsov, A. Barrett, M. Serreze, T. Pavlova, M. Holland, and W. N. Meier (2012), Trends in Arctic sea ice extent from CMIP5, CMIP3 and observations, *Geophys. Res. Lett.*, *39*, 7, doi:10.1029/2012GL052676.

Thorndike, A. S., and R. Colony (1982), Sea ice motion in response to geostrophic winds, *J. Geophys. Res.*, *87*, 5845–5852, doi:10.1029/JC087iC08p05845.

Tsukernik, M., D. N. Kindig, and M. C. Serreze (2007), Characteristics of winter cyclone activity in the northern North Atlantic: Insights from observations and regional modeling, *J. Geophys. Res.*, *112*, D03101, doi:10.1029/2006JD007184.

Ukita, J., M. Honga, H. Nakamura, Y. Tachibana, D. J. Cavalieri, C. L. Parkin-son, H. Koide, and K. Yamamoto (2007), Northern Hemisphere sea ice variability: Lag structure and its implications, *Tellus A*, *59*(2), 261–272, doi:10.1111/j.1600-0870.2006.00223.x.

Wallace, J. M., and P. V. Hobbs (2006), *Atmospheric Science: An Introductory Survey*, 2nd ed., pp. 504, Academic Press, San Diego, Calif.

Wu, B. Y., J. Wang, and J. E. Walsh (2006), Dipole anomaly in the winter Arctic atmosphere and its association with sea ice motion, *J. Clim.*, *19*(2), 210–225, doi:10.1175/jcli3619.1.

Yang, X.-Y., and X. Yuan (2014), The early winter sea ice variability under the recent Arctic climate shift, *J. Clim.*, *27*(13), 5092–5110, doi:10.1175/JCLI-D-13-00536.1.